

Monte Carlo Simulation of Sugar Synthesis on Icy Dust Particles Intermittently Irradiated by UV in a Protoplanetary Disk

Hitoshi Takehara^{1,2}, Daigo Shoji³, and Shigeru Ida¹

¹ Earth-Life Science Institute, Tokyo Institute of Technology, Meguro-ku, Tokyo 152-8550, Japan

² Department of Earth and Planetary Sciences, Tokyo Institute of Technology, Meguro-ku, Tokyo 152-8551, Japan

³ Institute of Space and Astronautical Science, Japan Aerospace Exploration Agency, Chuo-ku, Sagami-hara, Kanagawa 252-5210, Japan

DRAFT: March 15, 2022

ABSTRACT

Context. While synthesis of organic molecules in molecular clouds or protoplanetary disks is complex, observations of interstellar grains, analyses of carbonaceous chondrites, and UV photochemistry experiments are rapidly developing and providing constraints on and clues to the complex organic molecule synthesis in space. It motivates us to construct a theoretical synthesis model.

Aims. We develop a new code to simulate global reaction sequences of organic molecules to apply it for sugar synthesis by intermittent UV irradiation on the surface of icy particles in a protoplanetary disk. Here we show the first results of our new simulation.

Methods. We apply a Monte Carlo method to select reaction sequences from all possible reactions, using the graph-theoretic matrix model for chemical reactions and modeling reactions on the icy particles during UV irradiation.

Results. We here obtain the results consistent with the organic molecules in carbonaceous chondrites and obtained by the experiments, however, through a different pathway from the conventional formose reactions previously suggested. During UV irradiation, loosely-bonded O-rich large molecules are continuously created and destroyed. After UV irradiation is turned off, the ribose abundance rapidly increases, through the decomposition of the large molecules with break-ups of O-O bonds and replacements of C-OH by C-H to reach O/C = 1 for sugars. The sugar abundance is regulated mostly by the total atomic ratio H/O of starting materials, but not by their specific molecule forms. Deoxyribose is simultaneously synthesized, and most of the molecules end up with complex C-rich molecules.

Key words. Protoplanetary disks — Meteorites, meteors, meteoroids — Astrochemistry — Planets and satellites: formation

1. Introduction

In carbonaceous chondrites, polyhydroxylated compounds, and sugar derivatives, including sugar alcohols (reduced sugars) or sugar acids (oxidized sugars), were detected (Cooper et al. 2001; Cooper & Rios 2016), in addition to amino acids and nucleobases (Martins et al. 2008, 2015). Recently the detection of ribose (which is a sugar $C_k(H_2O)_k$ with $k = 5$; 5-C sugars) in meteorites was also reported (Furukawa et al. 2019). According to the findings, UV photochemistry experiments (Meinert et al. 2016; Nuevo et al. 2018) have been done to explore a possibility of sugar synthesis on the surface of icy dust particles in the interstellar or protoplanetary disk environments. They successfully produced ribose, deoxyribose and related sugars in the UV irradiated products formed from simple molecules. These findings suggest a possible hypothesis that these molecules were synthesized in molecular clouds or protoplanetary disks and delivered to the Earth (Oró 1961; Chyba & Sagan 1992).

Meinert et al. (2016) performed a photochemistry experiment by UV with 10 eV on a plate initially composed of CH_3OH , H_2O and NH_3 at 78 K which mimics the interstellar/protoplanetary icy dust surface environments, and reported that many kinds of sugars were synthesized, including ribose, in the final products at room temperature after UV is turned off. The authors suggested that the diverse sugar molecules are formed by formose-type reactions (Fig. 1). Formose-type reactions are well known as the bottom-up reaction for sugar synthe-

sis by aldol condensations to produce various molecules with linear and branched structures. However, there is no clear evidence in their experiment that sugars are formed mostly from formose-type reactions. Another similar experiment on sugar synthesis (except at 12 K instead of at 78 K) reported the detection of deoxysugars in the UV photochemistry products (Nuevo et al. 2018). In general, deoxysugars are not synthesized via formose-type reactions (Butlerow 1861; Breslow 1959). Since deoxy-sugar derivatives are also detected in meteorites (Cooper et al. 2001; Nuevo et al. 2018), a different reaction from formose-type reactions may also contribute to the synthesis of sugar molecules on icy dust particles.

In this paper, we focus on synthesis pathways of sugars or related molecules on the UV-irradiated surface of icy particles in relatively warm temperature (~ 50 – 100 K) environments such as in a protoplanetary disk. Particles occasionally diffuse to a highly upper layer of the disk to receive UV radiation from the host star, while for most of the time, the particles stay in the disk regions where UV radiation is shielded (Ciesla & Sandford 2012, also see Fig. 2). Each UV irradiation experiment would correspond to a full cycle of travels of the icy particle out of and back to the UV shielded region; UV photon flux for the disk environments may be up to 10^2 times higher than that for diffuse interstellar clouds and up to 10^5 times higher than that for cold dense interstellar clouds (Ciesla & Sandford 2012; Nuevo et al. 2018). In these UV irradiation experiments, the photochemical products were heated up to room temperature. It is not clear

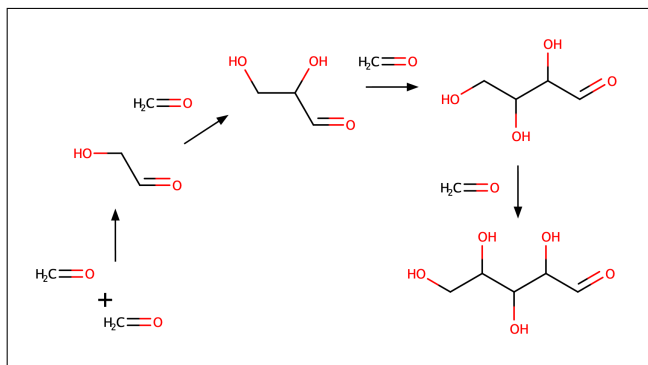


Fig. 1. Schematic diagram of typical formose-type reactions.

when the detected sugar molecules were synthesized, during UV irradiation or after that at room temperature.

We will show in this paper that chemical reactions of UV photochemical products significantly proceed after the UV irradiation is turned off. We will also show the products do not substantially depend on temperature after UV irradiation, as long as the temperature is in a rather broad range of ~ 10 – 1000 K.

In order to identify the reaction pathways to form complex organic molecules such as sugars, we employ computational simulations. In the computational studies of the synthesis of complex organic molecules on the surface of interstellar icy particles, the rate equation method has been often used (e.g., Chang & Herbst 2016; Garrod 2019; Jin & Garrod 2020). In these studies, setting target molecules (for example, methyl formate CH_3OCHO , dimethyl ether CH_3OCH_3 , acetaldehyde CH_3CHO , and methanol CH_3OH), a reaction network is set up based on the data of the reaction rate coefficients. Because cold environments, where most molecules are not sufficiently mobile, are often considered, a chemical kinetic model on the dust surface is sometimes combined with the reaction network model (Chang & Herbst 2016). In the kinetic model, the surface and the bulk of icy particles are divided into sites and Monte Carlo calculation is applied for molecule hopping from one site to another using an Arrhenius-type exponential probability with the hopping barrier potential energy.

Because we consider relatively warm environments with $T \sim 50$ – 100 K, we do not adopt such spatially limited kinetics and for simplicity we assume that all the species can interact with one another. Instead, we apply the Monte Carlo approach for chemical reactions without preparing a reaction network. To construct the Monte Carlo chemical-reaction scheme, we utilize a graph-theoretic matrix framework to represent molecules and chemical reactions that was originally developed by Dugundji & Ugi (1973) (Sect. 2.1). The matrix model has been used to find pathways to synthesize target products often for industrial purposes in the past studies (e.g., Dugundji & Ugi 1973; Habershon 2015, 2016; Kim et al. 2018; Ismail et al. 2019). The method used in Dugundji & Ugi (1973) is “backward,” in which reactants were investigated from target molecules. Habershon (2015, 2016) and Ismail et al. (2019) considered “forward” path (from reactants to targets). These works evaluate each synthesis referencing basal chemical reactions confirmed in laboratory experiments.

Although the database that registers reactions in laboratory experiments is very useful to assess synthesis paths, our primary purpose is to investigate how sugars (in particular, ribose) are synthesized in a broad range of conditions (environments) from

the protoplanetary disk to the early Earth. Thus, in this work, we try to evaluate chemical reactions without the reaction database. We do not restrict our study to only sugar synthesis, but also the synthesis of photochemical products in general including sugar alcohols, deoxysugars, and even Insoluble Organic Matter (IOM) that have been found in carbonaceous chondrites. We estimate the relative abundance of sugars, sugar alcohols, and deoxysugars and study in a general manner. In order to achieve this, we need a global survey in parameter space, so that we use the method without using the pre-registered reaction database. In this sense, our approach is a forward-type model and we perform Monte Carlo calculations with an Arrhenius-type exponential weighting (Sect. 2.2).

Another forward-type method without a database is quantum chemistry calculation. For Miller-type amino acids synthesis (Miller 1953, 1955), the quantum chemistry simulations were applied (Wang et al. 2014; Saitta & Saija 2014). Quantum chemistry calculations can evaluate synthesis paths of molecules accurately, and they have been widely used in the field of chemistry. Because reactions occur freely without preordained reaction coordinates or elementary steps, new reaction pathways can be discovered only by setting initial molecules and simulation environments. Wang et al. (2014) used an *ab initio* nanoreactor with repeated high pressure by a virtual piston that is equivalent to $\sim 10^4$ K and found a new pathway to form glycine. Saitta & Saija (2014) performed the calculation at 400 K and argued that electric field accompanied with the electric discharge is a key factor for glycine formation. In the work with the graph-theoretic method, Kim et al. (2018) also used quantum chemistry calculation for kinetic analysis of each reaction.

Quantum chemistry calculation is a commonly-used powerful tool to study the details of known reactions in given environments. However, interstellar/interplanetary complex organic molecule synthesis is complicated multi-step reactions with not well-known starting species in poorly understood environments. To explore it, broad enough parameter surveys are required. Quantum chemistry calculation’s cost would be too high for such surveys.

The synthesis of organic molecules (for example, sugars) in space is a complex process in a broad range of thermal and non-thermal conditions, while high-resolution analyses of organic molecules in carbonaceous chondrites, UV chemistry experiments, and quantum chemistry calculations are developing. Theoretical discussions on organic molecule synthesis in molecular clouds also have become active according to increasing detection of organic molecules by radio observations such as ALMA. This situation may be similar to exoplanet studies in the 1990s and the 2000s when the diverse mass-orbit distributions of exoplanets emerged. At that time, we pioneered the planet population synthesis model (Ida & Lin 2004), which has been substantially improved by our and others papers (e.g., Ida & Lin 2005; Moradasini et al. 2009; Ida & Lin 2010; Ida et al. 2013; Alibert et al. 2013; Benz et al. 2014). Multi-layered complex processes in planet formation were individually modeled to be combined to a global sequential model, in order to explain the existing observational data, predict the future data, constrain the theoretical models, and clarify missing pieces in the planet formation theory. Although the simplified prescriptions or parameterization in the model may introduce some ambiguity, the substantially lowered calculation costs enabled broad parameter surveys. Applying the concept of the planet population synthesis model for organic molecule synthesis in space, we develop a global chemical reaction simulation scheme that links the theory with the findings in carbonaceous chondrites and the experimental re-

sults. Restricting our simulation to the exploration of a global picture of synthesis pathways of sugars or related molecules in a specific environment, intermittent UV irradiation on the surface of icy particles in a protoplanetary disk, we introduce simplifications/assumptions with a Monte Carlo method to select reaction sequences (without quantum chemistry calculations) to accelerate the calculation substantially enough to follow global reaction sequences of sugar synthesis and survey a broad range of parameters. The details are explained below.

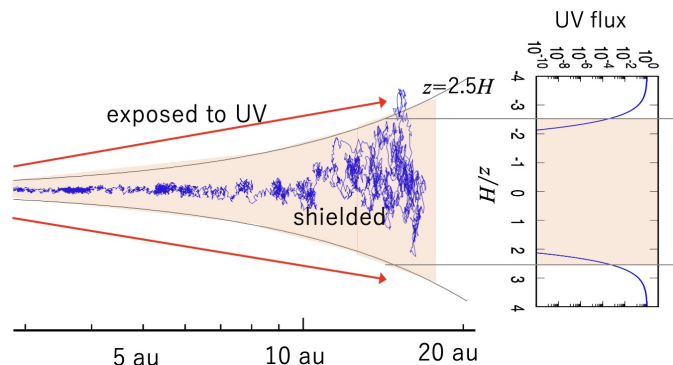


Fig. 2. A schematic illustration of a trajectory of an icy particle in a turbulent protoplanetary disk. The trajectory is represented by the zigzagged blue line. The shaded region represents a typical UV-shielded vertical height $|z| < 2.5H$, where H is the disk scale height. The right panel shows a typical vertical (z) attenuation of UV from a central star by the protoplanetary disk gas. The particle trajectory is simulated by the method of Okamoto & Ida (2022) with the effect of particle growth based on Sato et al. (2016). The particle is released at 15 au on the mid-plane and its orbit evolves by diffusion induced by the disk turbulence and inward advection due to gas drag.

Our new Monte Carlo chemical-reaction scheme with the graph-theoretic matrix framework is a forward-type method with a low computational cost. Although the availability of our scheme has limitations in reaction conditions, our scheme is available for the reaction sequences on icy dust particles intermittently irradiated by UV in warm environments that we are concerned with. The limitations and assumptions of our model are as follows:

1. We consider icy particles in a protoplanetary disk. Young T Tauri stars generally emit intense FUV (6–13.6 eV) and EUV (13.6 eV or more) radiation (Armitage 2013, and references therein). The particles are stirred by the disk turbulence. When they are occasionally pumped over the scale height, they are exposed to the UV flux and molecules on the icy surface are photo-dissociated by UV (Ciesla & Sandford 2012). Because we consider the high-energy UV, we neglect UV absorption dependence on molecules (Sect. 2.3).
2. We consider “warm” regions with $T \sim 50$ –100 K in the disk. While only H can move on the surface of the icy particles in the interstellar molecular clouds at the cold environments with $T \sim 10$ K (e.g., Jin & Garrod 2020), we assume that in the warm environments, molecules and radicals created by relatively strong UV irradiation move on the surface by diffusion to react with one another without desorption from the surface (Sect. 2.2).

Figure 2 schematically illustrates the situation that we consider in this paper. An icy particle at the outermost region in the protoplanetary disk is initially small enough to be coupled with disk

gas turbulence. It is occasionally stirred by the turbulence to the upper layer to be exposed to UV radiation from the host star. After the particle grows to a pebble size, the particle motion is confined to the region near the mid-plane where it is shielded against UV radiation (also see Bergner & Ciesla 2021).

The organic molecule synthesis on dust particles in interstellar clouds occurs in cold ($T \sim 10$ K) and lower UV flux environments. Diffusion of light elements on the dust surface would be a dominant process in the cold environments. Because the synthesis timescale would be much longer in the lower UV flux, interactions between the gas phase and the dust surface would play an important role. We do not address the simulation for the interstellar clouds in this paper, which is left for future study, because the main purpose of this paper is to demonstrate that our new approach has good potential to study global features of synthesis of complex organic molecules in astronomical environments with inexpensive computational costs.

2. Method

To construct our new simulation scheme, we utilize the graph-theoretic matrix model for molecules and their chemical reactions that was originally proposed in the 1970s by Dugundji & Ugi (1973). Adding a Monte Carlo scheme to the classical matrix model, we construct a new forward-type scheme for chemical reactions for organic synthesis, with particular interests in the synthesis of ribose and related sugars in space. The classical matrix model is summarized in Sect. 2.1. Our new Monte Carlo scheme is explained in Sect. 2.2, and the representation of UV irradiation is discussed in Sect. 2.3.

2.1. A Graph-theoretic Matrix Model to Represent Molecules and Chemical Reactions

A molecule with n atoms can be represented by a $n \times n$ matrix \mathbf{B} ; a non-diagonal element $B_{ij} = B_{ji}$ ($i \neq j$) indicates the bond order between the atom A_i and atom A_j , and diagonal elements B_{ij} ($i = j$) are always zero for covalent bonds (Dugundji & Ugi 1973, also see Fig. 3). Chemical reactions can be regarded as changes in bond arrangements. If \mathbf{B}^R is a bond matrix for the reactant and \mathbf{B}^P is that for the product, the chemical reaction is represented by a reaction matrix $\mathbf{R} = \mathbf{B}^P - \mathbf{B}^R$, which is an (addition) operator acting on \mathbf{B}^R . The matrix element R_{ij} indicates the change of the bond order between atom A_i and A_j . Figure 3 shows one example of our calculation, the formation of one glycolaldehyde from two formaldehydes.

In the past studies, a backward approach from a targeted product was often adopted, and accordingly, \mathbf{R} represented one-pod reactions with many-bond changes. However, because we adopt a forward approach without pre-selecting targets, we restrict \mathbf{R} to the minimum change with cleavage of one existing bond and creation of one new bond; in the matrix representation, four lines (or arrays) have only one element of $R_{ij} = -1$ and that of $R_{ij} = +1$ (all the other R_{ij} are zero) as shown in Fig. 3. We randomly select one reaction matrix from all the possible candidates with weighted probabilities (Sect. 2.2) and apply \mathbf{R} to \mathbf{B}^R . We regard the products \mathbf{B}^P as the reactants \mathbf{B}^R of the next step of the reaction sequence. Starting from given initial molecules, we repeat these transformations until the reaction sequence reaches the maximum number of steps that we specify.

We modify the original matrix representation by separating hydrogen atoms from the matrix to a vector \mathbf{H} , because bonds with hydrogen are uniquely determined from the non-hydrogen

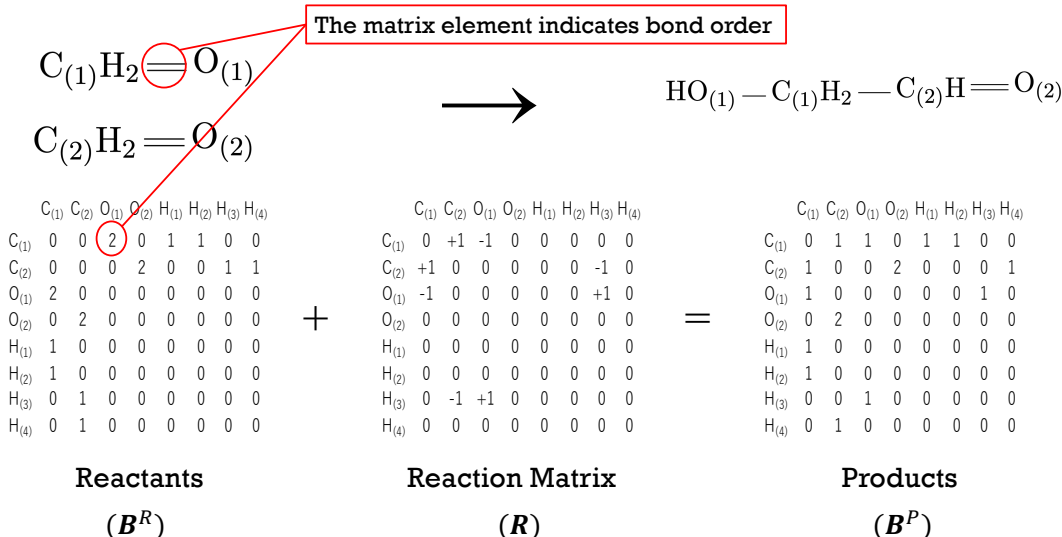


Fig. 3. An example of a reaction with the minimum bond change in the matrix form (from two formaldehydes to one glycolaldehyde).

matrix with the assumption that all the bonds are covalent. The separation of hydrogen-related bonds significantly reduces the matrix size and improves the calculation speed.

While the matrix representation can also treat ionic and coordination bonds, we only consider covalent bonds using non-diagonal elements, because most of the organic molecules are connected with covalent bonds and the effects of ionic bonds (electronegativity) on covalent bonds are reflected by empirical values of bond strengths between different atoms (Table 1 in Sect. 2.2). Carbon monoxide (CO) often plays an important role in chemical reactions. We tested the inclusion of CO, using the diagonal elements, to find that the simulated abundance of sugars hardly changes. Here we present the results by simpler and faster calculations without CO. Hydrogen bonds or other non-covalent bonding would play an important role in organic molecule synthesis in interstellar molecular clouds. As shown in Sect. 3.3, UV photo-dissociation is very efficient in the environments we consider, the predicted abundance of sugars does not significantly depend on starting molecule forms, but is regulated by initial atomic ratios. Therefore, the simulations in the most simple case in which only covalent bonds are considered would be enough for the main purpose of this paper, demonstration of the availability and potential of our new model. The inclusion of hydrogen or other non-covalent bonds is left for future study.

2.2. Weighting of Reaction Probability

As summarized at the end of Sect. 1, we adopt the following assumptions to highlight the advantage and availability of the computationally low-cost Monte Carlo calculations:

1. All the species interact with one another without a restriction due to spatial distance on the surface of the icy particles.
2. Desorption from the surface is neglected (a closed system).

Based on the above assumptions, we survey all the possible reactions with the minimum bond change (Sect. 2.1) at each step and select one reaction from the candidate reactions with the following Arrhenius-type weighting:

$$W = \exp\left(-\frac{E_a}{RT}\right), \quad (1)$$

where R is gas constant, T is the temperature of the environment, and E_a is an activation energy. The energy translation is

$$100 \text{ kJ mol}^{-1} \approx 1.2 \times 10^4 \text{ K} \approx 1.0 \text{ eV}. \quad (2)$$

For $E_a \sim 100 \text{ kJ mol}^{-1}$, the temperature dependence of W is weak at $T \gtrsim 10^4 \text{ K}$. In other words, the temperature dependence is pronounced for $T \lesssim 10^3 \text{ K}$.

The activation energy E_a can be calculated by *ab initio* density functional theory (DFT). However, we perform calculations of $10^5 - 10^6$ runs with different random numbers and each run consists of a 100 step reaction sequence with surveys of all the possible reactions at each step. We test 26 sets of different initial species for these runs (Table 2). Because DFT calculation has a high computational cost, if we use DFT calculations for the activation energy of all reactions, it significantly reduces the advantage of Monte Carlo simulation that is a global parameter survey with relatively low calculation cost.

To keep the advantage, in this work, we adopt a simpler weighting using the Evans-Polanyi's empirical law given by

$$E_a = \alpha \Delta H + \beta \approx \alpha \Delta D + \beta, \quad (3)$$

where ΔH is the enthalpy change during the reaction and α and β are almost constant for similar-type reactions. The DFT calculations (Michaelides et al. 2003; Wang et al. 2011; Sutton & Vlachos 2012) suggest that $\alpha \sim 0.6 - 1.0$ and $\beta \sim 1 - 2 \text{ eV}$ ($\sim 100 - 200 \text{ kJ mol}^{-1}$) for a wide variety of reactions. Because T is constant during a reaction in our setting, $\Delta H \approx \Delta D = D_P - D_R$ where D_R and D_P are the dissociation energies of reactants and products. The dissociation energy is approximated by a sum of the bond energies of all pairs of atoms in the molecules. We use the data of bond energies between a pair of atoms given in Sanderson (1976), which is listed in Table 1. For reaction selection in the Monte Carlo simulation, the weighting factor is normalized by $\sum_i W_i$, the total sum of all the possible reactions ($i = 1, 2, \dots, N$), to be a probability. Accordingly, $W \exp(\beta/RT)$ gives the same probability distribution of the reactions as W does, if β is a constant. Adopting $\alpha = 1$, the weighting is reduced to

$$W' = W \exp\left(\frac{\beta}{RT}\right) = \exp\left(-\frac{\Delta D}{RT}\right). \quad (4)$$

In this paper, we use W' in our Monte Carlo simulation.

We note that for the reaction to actually occur, $E_a \lesssim 30 RT$, which is equivalent to $E_a \lesssim 80 (T/300 \text{ K}) \text{ kJ/mol}$ (e.g., Rzepa 2021), is required. As we will show in Sects. 2.3 and 3.1.2, $E_a \ll RT$ in the UV irradiation phase in our simulations, and in the following non-UV phase in warm environments (“post UV phase”), $E_a \lesssim 0 \text{ kJ/mol}$ assuming Eq. (3), until peaked synthesis of sugars in the post UV phase. Thus the effect of the activation energy is negligible until the peaked sugar synthesis. While predicted reactions after the peaked sugar synthesis would be affected by the activation energy, it would contribute to longer preservation of sugars (for details, see Sect. 4.1).

In our prescription to calculate ΔD , where the dissociation energy is approximated by a sum of the bond energies of all pairs of atoms, the three-dimensional structure of molecules is not reflected. We will discuss this issue in terms of the cyclic and chain structure of sugars (Sect. 3.1.3).

In our simulations, we adopt UV irradiation with 10 eV, following Meinert et al. (2016). The UV energy of 10 eV is represented by an equivalent temperature $T = 10^5 \text{ K}$ for Eq. (4) (see Sect. 2.3), while thermal room temperature ($T = 300 \text{ K}$) is assigned to the post UV phase to mimic the Meinert et al. (2016)’s experiments (see the detailed discussion in Sect. 2.4).

Table 1. Bond dissociation energy taken from Sanderson (1976). The energy translation is $100 \text{ kJ mol}^{-1} \approx 1.2 \times 10^4 \text{ K} \approx 1.0 \text{ eV}$.

| dissociation energy | | dissociation energy | |
|---------------------|----------------------------|---------------------|----------------------------|
| H – H | 435.5 kJ mol ⁻¹ | C = C | 610.3 kJ mol ⁻¹ |
| C – C | 347.0 kJ mol ⁻¹ | O = O | 497.4 kJ mol ⁻¹ |
| O – O | 146.3 kJ mol ⁻¹ | C = O | 744.0 kJ mol ⁻¹ |
| C – H | 413.8 kJ mol ⁻¹ | | |
| O – H | 464.0 kJ mol ⁻¹ | C \equiv C | 836.0 kJ mol ⁻¹ |
| C – O | 357.4 kJ mol ⁻¹ | | |

Our prescription for Monte Carlo is summarised as follows:

1. At each step, we list up all the possible R_i ($i = 1, 2, \dots, N$) from B^R .
2. Using Table 1, ΔD_i is calculated for all of R_i .
3. The probability W'_i is calculated by Eq. (4) with the calculated ΔD_i and the given T of the environment.
4. Generating a random number with the weighting of W'_i , a particular reaction is selected and the corresponding R_i is applied for B^R to obtain B^P .
5. The product B^P is assigned to B^P for the next step and we go back to 1.

2.3. UV Irradiation

In our simulations, we adopt UV irradiation with 10 eV, following Meinert et al. (2016). The UV radiation energy of 10 eV corresponds to an equivalent temperature $\sim 1.2 \times 10^5 \text{ K} \sim 10^3 \text{ kJ mol}^{-1}$ (Eq. (2)). Because UV irradiation with 10 eV would result in the bond cleavage to create radicals rather than transition to a higher bond energy level, the wavelength dependence of UV absorption for individual molecules may not be sensitive (e.g., Limão-Vieira et al. 2003) and the representation of UV irradiation by $T = 10^5 \text{ K}$ would be a good approximation. While the radicals may stay on the icy surface, we assume that they can diffuse and interact with any other species on the surface (for liquid-like behavior of ice radiated by UV in this temperature range, see Tachibana et al. 2017).

Because E_a and ΔD for a minimum bond change are typically $< 500 \text{ kJ mol}^{-1}$, which is equivalent to $< 6 \times 10^4 \text{ K}$, for the minimum bond change reactions that we consider (see also Table 1), the weighting W given by Eq. (1) and W' given by Eq. (4) are ~ 1 for all of possible reactions under the UV irradiation. In other words, the energy of 10 eV UV irradiation, corresponding to $\sim 10^5 \text{ K}$, is sufficiently higher than the energy barriers of each reaction, and thus the activation energy is negligible in the UV irradiation phase.

In our fiducial simulation runs, we calculate $N_U = 70$ steps in the UV phase followed by $N_P = 30$ steps at 300 K without UV irradiation (Sect. 2.4). While steps in the 300 K phase represent time evolution, the interpretation of the UV phase needs to be careful. In our simulations, radicals are not explicitly treated. We formally assume that atoms are in covalent bonds, but their bonds are actually cleaved by UV. What we simulate is the equilibrium distribution of molecules that temporarily exist as very loosely bounded or that is expected to establish when UV irradiation flux decays. In this sense, UV phase calculation is equivalent to setting-up of initial conditions for the post-UV low-temperature evolution.

2.4. Parameter Settings

Table 2. Patterns of a set of initial conditions: species, H/O, and H/C ratios of starting materials. P1 is the fiducial set.

| | starting materials | H/O ratio | H/C ratio |
|-----|---|-----------|-----------|
| P1 | 7 CH ₂ O, 20 H ₂ O | 2.00 | 7.71 |
| P2 | 4 CH ₂ O, 3 CO ₂ , 4 H ₂ | 1.60 | 2.29 |
| P3 | 5 CH ₂ O, 2 CO ₂ , 9 H ₂ O | 1.56 | 4.00 |
| P4 | 2 CH ₃ OH, 5 CO ₂ , 17 H ₂ O | 1.45 | 6.00 |
| P5 | 2 CH ₂ O, 5 CO ₂ , 25 H ₂ O | 1.46 | 7.71 |
| P6 | 7 CO ₂ , 32 H ₂ O, 3 H ₂ | 1.52 | 10.00 |
| P7 | 7 CH ₂ O | 2.00 | 2.00 |
| P8 | 13 CH ₂ O, 14 H ₂ O | 2.00 | 4.15 |
| P9 | 10 CH ₂ O, 17 H ₂ O | 2.00 | 5.40 |
| P10 | 7 CH ₂ O, 17 H ₂ O | 2.00 | 6.86 |
| P11 | 7 CH ₂ O, 24 H ₂ O | 2.00 | 8.86 |
| P12 | 7 CO ₂ , 21 H ₂ O, 14 H ₂ | 2.00 | 10.00 |
| P13 | 7 CH ₂ O, 17 H ₂ O, 3 H ₂ | 2.25 | 7.71 |
| P14 | 7 CH ₂ O, 4 H ₂ O, 3 H ₂ | 2.55 | 4.00 |
| P15 | 7 CH ₂ O, 10 H ₂ O, 4 H ₂ | 2.47 | 6.00 |
| P16 | 7 CH ₂ O, 14 H ₂ O, 6 H ₂ | 2.57 | 7.71 |
| P17 | 7 CH ₂ O, 18 H ₂ O, 6 H ₂ | 2.48 | 8.86 |
| P18 | 7 CH ₃ OH, 20 H ₂ O | 2.52 | 9.71 |
| P19 | 7 CH ₃ OH, 24 H ₂ O | 2.45 | 10.86 |
| P20 | 7 CH ₂ O, 4 H ₂ | 3.14 | 3.14 |
| P21 | 7 CH ₃ OH, 7 H ₂ O | 3.00 | 6.00 |
| P22 | 7 CH ₃ OH, 11 H ₂ O, 3 H ₂ | 3.11 | 8.00 |
| P23 | 7 CH ₂ O, 16 H ₂ O, 5 H ₂ | 3.04 | 10.00 |
| P24 | 7 CH ₂ O, 1 H ₂ O, 6 H ₂ | 3.50 | 4.00 |
| P25 | 7 CH ₂ O, 5 H ₂ O, 9 H ₂ | 3.50 | 6.00 |
| P26 | 7 CH ₂ O, 9 H ₂ O, 12 H ₂ | 3.50 | 8.00 |

While our primary purpose is to investigate how complex organic molecules are generally synthesized on the surface of icy dust particles by intermittent UV irradiation in the protoplanetary disks, we define fiducial parameters in our simulations as those corresponding to Meinert et al. (2016)’s experiments. This is because quantitative comparisons with the experiments would be important to construct and constrain the theoretical model. Meinert et al. (2016) suggested formation of ribose by formose-

type reactions. However, they used methanol as starting materials, rather than formaldehyde because of its difficulty of treatment. In numerical simulations, such difficulty does not exist and we use 7 formaldehyde molecules and 20 water molecules ($7 \text{ CH}_2\text{O} + 20 \text{ H}_2\text{O}$) as fiducial starting materials to compare the suggested formose-type reactions with the sugar synthesis paths obtained by our numerical simulation. In Sect. 3.3, we will show that a specific choice of starting molecule structures does not affect the peak abundance of ribose in the post UV phase.

In organic photochemistry experiments, as in Meinert et al. (2016), the samples are warmed up to room temperature after UV irradiation for the spectroscopic analysis. Because the warmed-up phase may induce important reactions for sugar synthesis, we consider two phases in our simulation, the UV phase ($T = T_U$) and the post UV phase ($T = T_p$). Because Meinert et al. (2016) used 10 eV UV and set the sample at room temperature for the analysis, we define fiducial temperatures as $T_U = 10^5 \text{ K}$ and $T_p = 300 \text{ K}$.

In Sect. 1, we mentioned that our simulation setting would be justified for $T_p \sim 50\text{--}100 \text{ K}$. We show in Sect. 3.2 that the predicted sugar abundance is almost the same for $T_p \lesssim 10^3 \text{ K}$ in our simulations. Our simulation setting that assumes preservation of all of the atoms breaks down for the room temperature or more, because volatile molecules such as H_2O sublimate. However, the complex organic molecules would remain to be analyzed. Accordingly, we set $T_p = 300 \text{ K}$ in most of our simulations.

For each set of initial molecules, we repeat $n_{\text{run}} = 10^5\text{--}10^6$ runs of $N_U = 70$ step reactions in the UV phase and $N_p = 30$ step reactions in the post UV phase. In each run, a random number sequence is different. We will show that the results are not affected by the choices of T_U and T_p as long as $T_U \gtrsim 10^4 \text{ K}$ and $T_p \lesssim 10^3 \text{ K}$. As shown in Sect. 3, the sugar synthesis does not depend on N_U and N_p as long as $N_U \gtrsim 40$ and $N_p \gtrsim 20$. For safety, we adopt $N_U = 70$ and $N_p = 30$.

We tested 26 sets with different starting materials that are summarized in Table 2. We first show the results of simulations with the fiducial initial materials and parameters in detail (set P1). After that, we investigate the dependence of sugar synthesis on temperature and starting materials. We compare the predicted relative abundance of sugars, sugar alcohols, and deoxysugars with the experimental results.

3. Results

The synthesis pathway of sugars found in our simulations is the formation of large O-rich molecules randomized by UV irradiation followed by irreversible break-ups of the O-O bonds to be replaced by C-O/O-H and replacements of -OH by -H in the post UV phase. It is a very different pathway from the conventional step-by-step bottom-up pathway such as formose-type reactions¹. Figure 4 is a schematic illustration of the two pathways. Below, we show the details of every part of the pathway that we find, based on the detailed numerical results. The schematic illustration helps understand the whole picture of the pathway.

¹ For the synthesis of complex organic molecules in interstellar clouds, a scenario of formation of large molecules by radical-radical interactions followed by sputtering and photofission was also proposed (e.g., Sorrell 2001), although UV and temperature environments are different from those in the present paper.

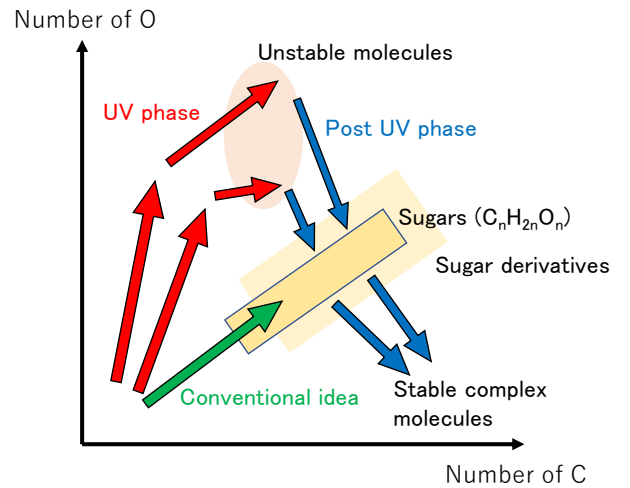


Fig. 4. Sugar synthesis pathways shown by our simulation (the red and blue arrows) and by the conventional formose-type reactions (the green arrows). The horizontal and vertical axes are the numbers of carbon and oxygen atoms contained in molecules, respectively.

3.1. Simulation for Fiducial Parameters

We show the abundance evolution of 4-C and 5-C sugars as a function of a reaction step. In this paper, the “abundance” is defined as the frequency for targeted sugar molecules to exist at each step. If targeted molecule k -C sugars exist at the n_{step} -th step in $n_{k\text{-C}}$ runs out of the total runs n_{run} , the abundance at n_{step} is given by

$$P_k = n_{k\text{-C}}/n_{\text{run}}. \quad (5)$$

Here “sugars” that we count are the molecules with the cyclic or open-chain structure shown in Fig. 5. We do not count k -C sugars in the furanose form (k -membered ring), because most of k -C sugars existing in the cyclic form have pyranose structure ($(k+1)$ -membered ring) and the definition should be simple to avoid ambiguity.

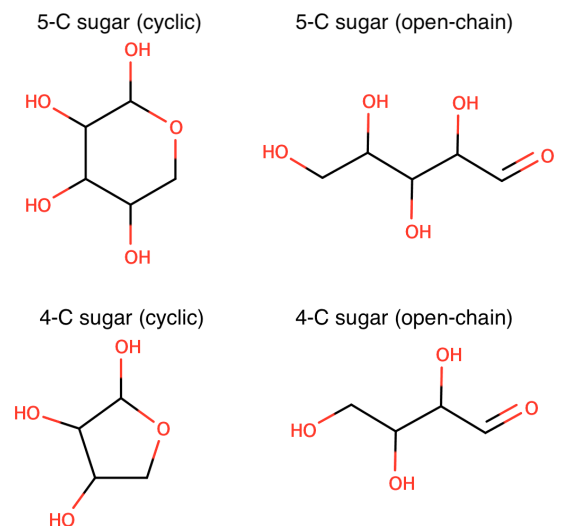


Fig. 5. Chemical structures of k -C sugars ($k = 4, 5$) that we count to calculate the abundance. We count both the (pyranose) cyclic and open-chain forms.

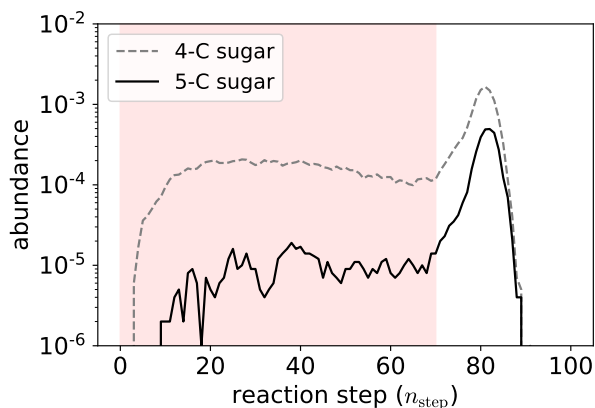


Fig. 6. The abundances of 4-C and 5-C sugars as a function of a reaction step for the fiducial set (P1), starting from 7 CH₂O and 20 H₂O, and temperature of $T_U = 10^5$ K and $T_p = 300$ K. The abundance is defined by Eq. (5). The grey dashed line and black solid line are for 4-C and 5-C sugars, respectively. The red area corresponds to the UV phase.

Figure 6 shows the results for fiducial parameters: starting from 7 CH₂O and 20 H₂O, $T_U = 10^5$ K (10 eV of UV irradiation) and $T_p = 300$ K. The total runs are $n_{\text{run}} = 10^6$. Synthesis of 4-C and 5-C sugars begin after a few and ~ 10 steps, respectively, and their abundance keeps an almost constant value from $n_{\text{step}} \sim 30$ –40 through the end of UV phase ($n_{\text{step}} = 70$). In the post UV phase at 300 K ($71 \leq n_{\text{step}} \leq 100$), the abundance of 4-C and 5-C sugar rapidly increases until $n_{\text{step}} \sim 80$ followed by quick decay. As we will discuss, the final rapid decay would not be realistic, while the evolution until the peaked sugar synthesis may be actually realized.

3.1.1. Large Molecules Formed in the UV Phase

As we discussed in Sect. 2.3, the simulated evolution in the UV phase does not necessarily mean actual time evolution, but it rather shows the relaxation to the equilibrium distribution of molecules that is regarded as the initial conditions for the post UV low-temperature evolution. In the fiducial case, thanks to the initially existing formaldehyde, 4-C and 5-C sugars are quickly formed. However, because the equivalent energy with $T_U = 10^5$ K is higher than the bond energy changes associated with the minimum bond change reactions ($\lesssim 350$ kJ mol⁻¹; Table 1), the weights of Monte Carlo calculations, $\exp(-\Delta D/828$ kJ mol⁻¹) for $T_U = 10^5$ K, are ≈ 1 for all of the possible minimum bond change reactions from the molecules at each step. Accordingly, UV irradiation randomly rearranges chemical bonds by repeated cleavage and combination of all possible reactions, independent of their bond strength. As a result, UV generates a variety of molecule sizes.

Figure 7 shows the distribution of molecules at each step on the plane of C and O atom numbers of the molecules. The circle sizes represent the abundance. Because seven C atoms initially exist, the distribution is truncated at $C = 7$. While small molecules also exist, the distribution spreads and large molecules are synthesized as n_{step} proceeds, which have some chain or branched structures consisting of the sequences of bonds of carbon and oxygen atoms. For $n_{\text{step}} \gtrsim 40$ in the UV phase, the distribution reaches an equilibrium. Sugar molecules are also formed in this phase, but they are decomposed immediately due to random rearrangements of bonds. For $n_{\text{step}} \gtrsim 40$ in

this UV phase, these repeated cleavage and combination balance and the sugar abundance are kept almost constant.

3.1.2. Sugar Synthesis in the Post UV Phase

After UV irradiation is turned off and the T is switched to 300 K ($n_{\text{step}} \geq 71$), the Monte Carlo calculation is drastically changed. The weight becomes $\exp(-\Delta D/2.48$ kJ mol⁻¹) and reactions are sensitively contrasted by the weights. Accordingly, the abundance of 4-C and 5-C rapidly increases, as explained below.

The dissociation energy of O-O bonds is smaller than that of C-O bonds by ~ 210 kJ mol⁻¹ and that of O-H bonds by ~ 320 kJ mol⁻¹ (Table 1). For the reaction including this bond change, ΔD is usually $\sim -(260$ – $350)$ kJ mol⁻¹ and the reaction probability is higher than the other reactions by a huge factor. Therefore, the reaction to break O-O bonds are predominantly selected by the Monte Carlo calculation, and the existing O-O bonds are replaced by the stronger bonds one after another until all of the O-O bonds are broken. Molecules are rapidly converted to more stable structures.

The top panel of Fig. 8 shows ΔD at each reaction step. The blue dots are the distributions of 10^3 runs in set P1. A typical path of ΔD for a reaction sequence of 5-C sugar synthesis and that without sugar formation are also shown. In a few steps after the termination of the UV irradiation ($n_{\text{step}} = 70$), only the reaction with $\Delta D = -346$ kJ mol⁻¹ is selected. The reaction is the break-up of O-O bonds by attacks of H₂: $\text{H}_2 + \text{O-O} \rightarrow 2 \text{OH}$ (Table 1). For $n_{\text{step}} \sim 75$ –85, other reactions to break up O-O bonds, $\text{C-H} + \text{O-O} \rightarrow \text{C-O} + \text{O-H}$ with $\Delta D = -261$ kJ mol⁻¹ and $\text{H-C-O-O} \rightarrow \text{C=O} + \text{O-H}$ with -291 kJ mol⁻¹, are also selected, in addition to the above reaction. The reaction of replacing C-OH by a stronger bond C-H with the formation of H₂O ($\Delta D = -85$ kJ mol⁻¹) also starts at $n_{\text{step}} \sim 75$ and continues through the end of the runs. As the break-ups of O-O bonds proceed, the molecule sizes decrease as shown in the panels $n_{\text{step}} = 70, 75, 80$ and 85 in Fig. 7.

In this phase, the abundance of 4-C and 5-C sugars rapidly increases until $n_{\text{step}} \sim 80$, as shown in Fig. 6. In the post UV phase, large unstable molecules with $\text{O/C} > 1$ formed in the UV phase are decomposed by the break-ups of O-O bonds, irreversibly decreasing the O/C ratio and probabilistically producing sugars.

Figure 8 c shows the evolution of O/C of molecules composed of four carbon atoms or more. During the UV phase, O/C values are distributed broadly at ~ 1.0 – 3.0 . Because H/C is distributed at ~ 1.5 – 2.5 , as shown in Fig. 8 b, a small fraction of the molecules is in the state of sugars, $\text{O/C} = 1$ and $\text{H/C} = 2$. Soon after the UV irradiation is turned off, the O/C distribution is converged with the decrease of its mean value through the break-ups of O-O bonds and the replacements of -OH by -H, while the H/C distribution is kept constant. As a result, molecules arrive at sugars with $\text{O/C} = 1$ and $\text{H/C} = 2$ with small but non-negligible probability ($\sim 5 \times 10^{-4}$). Figure 9 shows one example of sugar synthesis pathways.

The Evans-Polanyi's empirical law with DFT calculations (Eq. 3) suggests that the activation energy can be neglected for the reactions with $E_a \lesssim 80 (T/300 \text{ K})$ kJ/mol (Sect. 2.2). For $\alpha = 1$, this condition corresponds to $\Delta D \lesssim [80 (T/300 \text{ K}) \text{ kJ/mol} - \beta]$, which is ~ -20 to -120 kJ/mol at $T \approx 300$ K. Because the reactions including the O-O bond break-ups have $\Delta D \sim -350$ to -260 kJ mol⁻¹, it is likely that sugar synthesis by this process is not inhibited by its activation

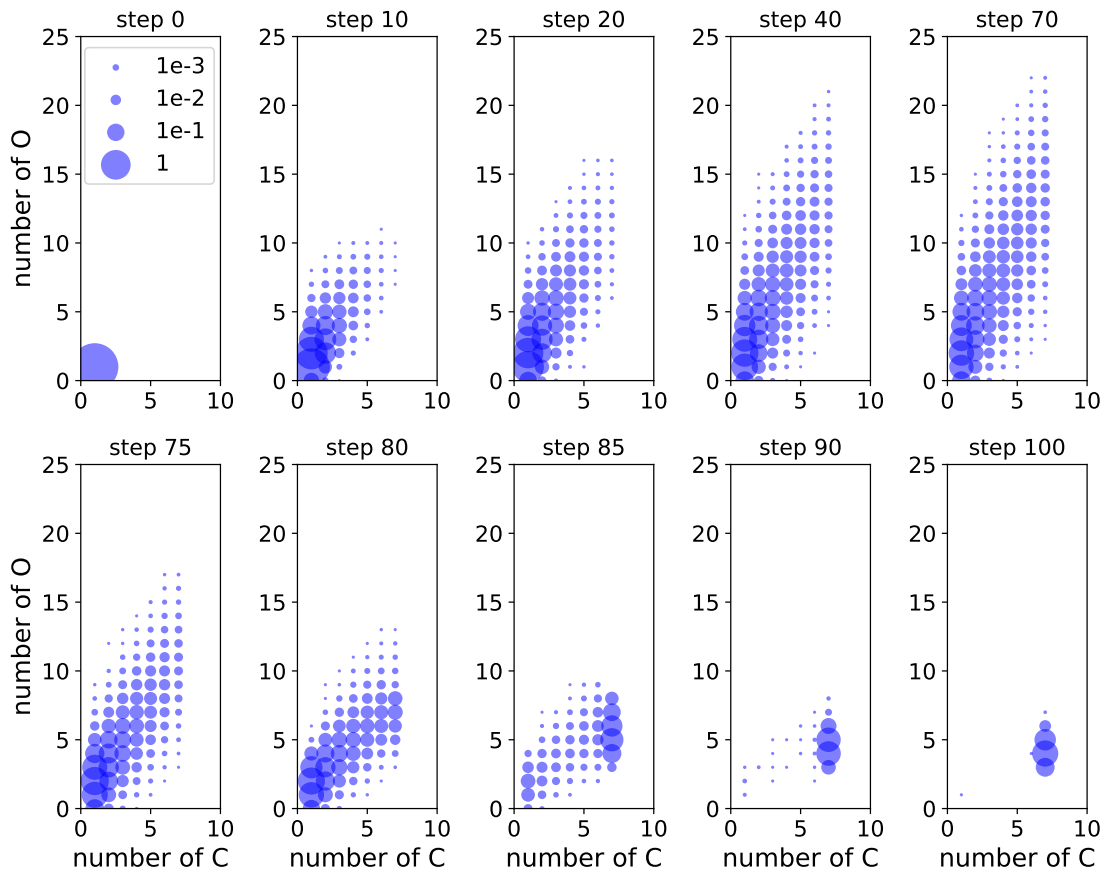


Fig. 7. Evolution of the molecule distribution for the fiducial parameters. The horizontal and vertical axes indicate the number of C and O in the individual molecules at each step. All of the molecules with different numbers of C and O at each step are plotted with the abundance (out of the total runs $n_{\text{run}} = 10^5$) represented by the circle sizes. The upper and lower panels show the evolution in the UV phase and the post UV phase, respectively.

energy. On the other hand, the replacements of -OH by -H with $\Delta D \sim -85 \text{ kJ mol}^{-1}$ may be marginal to occur.

In Sect. 3.2, we confirm that no sugar is synthesized in the case where $T = 300 \text{ K}$ is set in all steps. The formation of large O-rich molecules at $T \gtrsim 10^4 \text{ K}$ (corresponding to the energy $\gtrsim 1 \text{ eV}$) is a necessary condition for the sugar synthesis in our setting. Thus, UV radiation plays an important role in the enhanced synthesis of sugars in the post UV phase.

3.1.3. Preservation of Sugars

In our simulations, 4-C and 5-C sugar abundance is peaked at ~ 80 steps. After the peak, the replacements of -OH by -H continue and molecules become further O-poor ($O/C < 1$), as shown in Fig. 8 c. Because $O/C = 1$ for sugars, the sugar abundance rapidly decreases. After the peak, H/C also starts decreasing through reactions of replacing C-H bonds by C-C bonds, because H is taken by O to form H_2O with high bond strength. In the case where three or four-membered ring structures are allowed (the dark color dots), we find more O-poor ($O/C \ll 1$) molecules are formed. We will come back to this final evolution that could be related to formation of IOM in Sect. 4.2.

Because the reaction of replacing -OH by -H has $\Delta D = -85 \text{ kJ mol}^{-1}$ in our prescription (Table 1), the activation energy may not be low enough to be neglected and it is affected by the three-dimensional structure of molecules. Accordingly, we need

a more careful discussion on the decomposition of sugars found in our simulations.

Sugars in a solution have two types of forms, the open-chain and the cyclic forms. It is empirically well known that the cyclic form is more stable than the open-chain form, and most sugars are in the cyclic form in a solution. Because sugars change a form in a solution, sugars can occasionally take the open-chain form and be decomposed, although the probability of the decomposition is small. As a result, the decomposition timescale is relatively long at room temperature. Dass et al. (2021) suggests that the cyclic form has lower energy by $\sim 10\text{--}30 \text{ kJ mol}^{-1}$ than the open-chain form and Azofra et al. (2012) suggests $\sim 50 \text{ kJ mol}^{-1}$. Because the two forms have similar dissociation energies in our prescription, the above energy difference should reflect the three-dimensional structure, which we do not take into account. The accurate value of this conversion energy is not clear enough for us to explicitly introduce to our simulation. The reaction of replacing -OH by -H has $\Delta D = -85 \text{ kJ mol}^{-1}$ and is marginal for the decomposition due to the activation energy. The additional energy decrease of $\sim 10\text{--}50 \text{ kJ mol}^{-1}$ for the cyclic form may result in the preservation of sugars against the -OH/-H replacement reactions.

In this paper, we adopt a stable-limit assumption that sugars formed at room temperature is quickly transformed into the more stable cyclic form to inhibit further decomposition by the -OH/-H replacements. Thereby, the peak values of sugar abundance

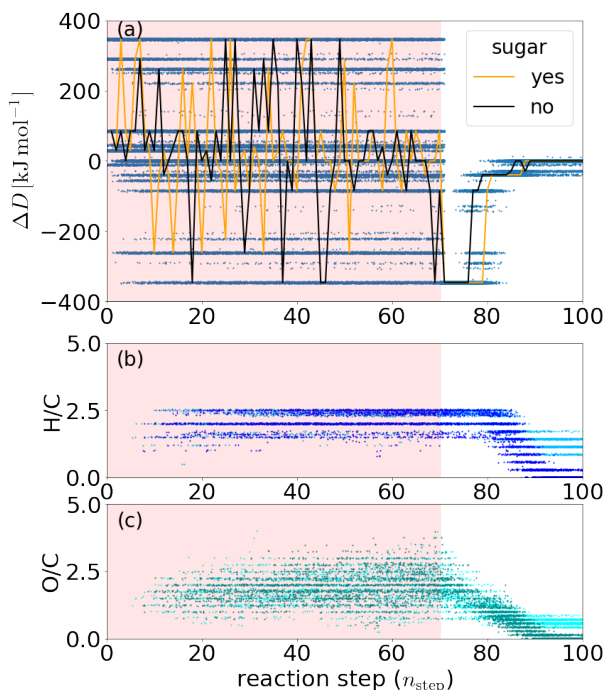


Fig. 8. The dissociation energy and associated composition changes of large molecules along reaction sequences in the UV phase ($n_{\text{step}} = 1-70$) and the post UV phase ($n_{\text{step}} = 71-100$). The top panel is (a) the distribution of ΔD selected by the Monte Carlo simulations at each step in 10^3 runs in set P1. The horizontal axis is a reaction step, and the vertical axis is ΔD in the unit of kJ mol^{-1} . The yellow and black lines are typical reaction sequences where 5-C sugar is formed and that without sugar formation, respectively. The middle and bottom panels show the distributions of (b) H/C and (c) O/C ratios of the molecules with four or more carbon atoms at each step in the 10^3 runs. The dark color dots indicate the results in the case allowing the formation of three or four-membered ring structures, and light color dots are the results with prohibiting their formation. For visual convenience, the dots with the same ΔD , H/C, and O/C at n_{step} are shifted slightly so that they do not overlap and clustered dots represent frequent events.

are used to compare with the experimental results (Sects. 3.4 and 3.5).

The large molecules prepared in the UV phase are decomposed into smaller molecules with fewer oxygen atoms by the break-up of O-O bonds and the -OH/-H replacements through many different paths. On the way of the reduction of oxygen atoms in molecules, a small fraction of the molecules happen to pass sugars and may be stabilized by the transformation to the cyclic form. In Fig. 8 a, we also plot the paths in which 5-C sugars are formed in the post UV phase as well as those without sugar synthesis. It shows that the paths are similar to each other, independent of whether sugars are synthesized or not, which suggests that the sugar synthesis is just by chance following the probability distribution. A more detailed preservation mechanism of synthesized sugars is left for future work.

3.2. Dependence on Temperature

In the fiducial runs, we set $T_U = 10^5$ K (10 eV of UV irradiation) and $T_p = 300$ K. Here, we show the peak sugar abundance with different T_U and T_p . Figure 10 a shows the peak values of 4-C and 5-C sugar abundances in the post UV phase as a function of T_U for the fixed $T_p = 300$ K. The peak abundances of 4-C and 5-

C sugars are 2×10^{-3} and $5-6 \times 10^{-4}$, respectively, independent of T_U for $T_U \gtrsim 10^4$ K. Figure 10 b shows the dependence on T_p for the fixed $T_U = 10^5$ K. Both abundances are the same for $T_p \lesssim 10^3$ K.

The typical bond energy difference $|\Delta D|$ is $\sim 10-350$ kJ mol^{-1} (Fig. 8 a), which corresponds to the temperature of about $10^3-3 \times 10^4$ K. When $T_U \gtrsim 10^4$ K, most of the reactions occur without a large difference in the probability and a similar distribution of molecules is prepared for the irreversible reactions in the post UV phase. On the other hand, when $T_p \lesssim 10^3$ K, which corresponds to $\lesssim 10$ kJ mol^{-1} , the reactions with $\Delta D \sim -350$ to -260 kJ mol^{-1} are continuously selected if the unstable O-rich molecules are remained. Thereby, the rapid increase of sugar abundance after UV irradiation is rather a universal event in a broad range of the environment temperature, but not a tuned event that occurs only at a specific temperature.

3.3. Dependence on Starting Materials

If sugars are synthesized by a step-by-step bottom-up pathway such as formose-type reactions, starting species would be important. However, in the sugar synthesis pathways that we have shown here, the equilibrium molecule distribution is established by the random bond arrangements by UV irradiation. We find that the peak abundance of sugars is regulated by atom ratios such as H/O and H/C, but not by specific starting species.

In order to understand how sugar abundance depends on starting materials, we performed runs in sets with a variety of starting materials listed in Table 2. The results are summarized in Fig. 11. The circles indicate H/O and H/C ratios of starting materials we tested, and the color contours indicate the peak value of 5-C sugar abundance in the post UV phase interpolated by the results with discrete values of H/O and H/C ratios. We find three important features.

The first one is that the sugar synthesis efficiency is mostly regulated by the H/O ratio. The peak value is obtained with $\text{H/O} \approx 2.0$ for a fixed H/C. As we showed, molecules convert to more stable structures with strong bonds in the post UV phase. Figure 12 shows the sugar abundance for three patterns (P1, P5, and P16 in Table 2). These patterns have the same H/C ratio ($= 7.71$) and different H/O ratio ($\text{H/O} = 2.00, 1.46, \text{ and } 2.57$ for P1, P5, and P16). The peak value in the post UV phase is the largest for $\text{H/O} \approx 2$. On the other hand, few sugars are synthesized in both the UV phase and the post UV phase for $\text{H/O} \approx 1.5$ (O-rich environment; P5). In this case, oxygen atoms are abundant at the initial state and most of the molecules formed in the UV phase include more oxygen than sugars, so that sugar synthesis is not efficiently induced in the UV phase. In the post UV phase, most carbon atoms combine with oxygen and they construct molecules without hydrogen, such as carbon dioxide, rather than carbon chains necessary for sugar synthesis, because C=O bonds are very strong. When the H/O ratio is high (H-rich environment; P16), in the post UV phase, most carbon atoms construct small carbohydrate molecules and oxygen atoms tend to form water molecules because the C-H bond is stronger than the C-O bond. It demonstrates that too oxidizing or reducing environment is not suitable for sugar synthesis.

Second, for $\text{H/O} > 2$, the abundance decreases as the H/C ratio increases from $\text{H/C} \approx 5$. Figure 13 shows the results of P20, P21, and P23 that have the same H/O ratio (≈ 3) but different H/C ratios; $\text{H/C} = 3.14, 6.00, \text{ and } 10.00$ for P20, P21, and P23, respectively. The peak value of the sugar abundance in the post UV phase is smaller for high H/C ratios (P23). We also

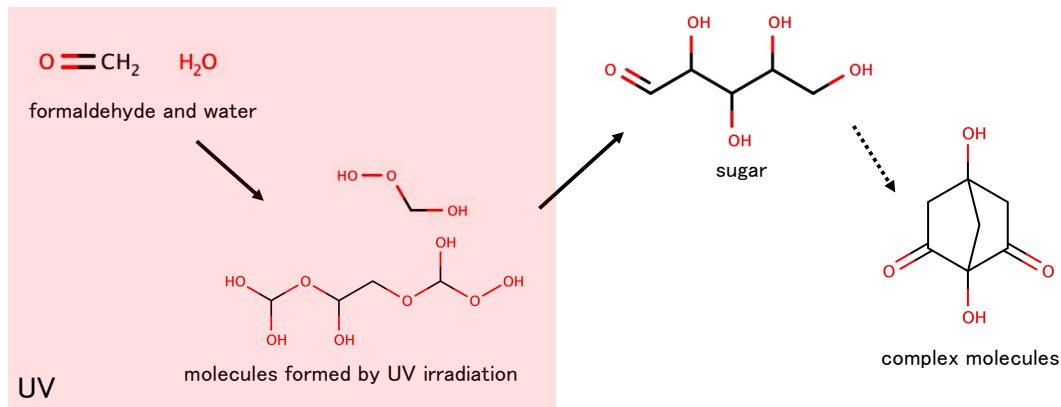


Fig. 9. One example of reaction paths of ribose synthesis. The red-shaded region represents the evolution during the UV phase and the non-shaded region shows the evolution in the post UV phase.

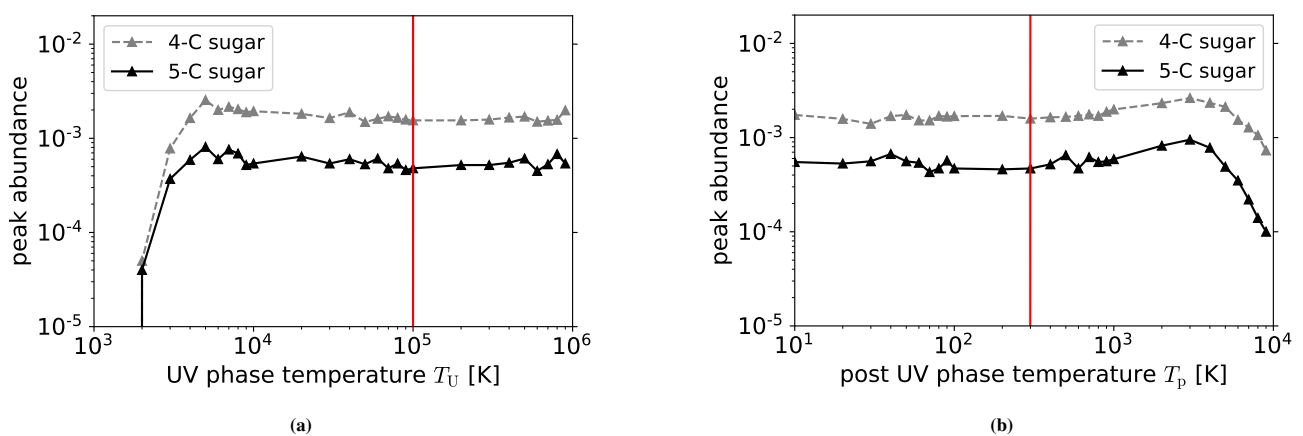


Fig. 10. The peak sugar abundances in the post UV phase for different temperatures when $n_{\text{run}} = 10^5$. We use fiducial starting materials. The left panel (a) shows the dependence on temperature of the UV phase when $T_p = 300$ K, and the right panel (b) shows the dependence on temperature of the post UV phase when $T_U = 10^5$ K. The grey dashed line and black solid line are for 4-C and 5-C sugars, respectively. Red lines indicate the positions of the fiducial temperatures.

note that the sugar abundance in the early UV phase is different, although it does not depend significantly on H/O (Fig. 12). For high H/C ratios, excess hydrogen atoms combine with carbon atoms and produce small hydrocarbons such as methane, preventing the molecules from becoming large with many carbon atoms. Even in the post UV phase, hydrogen atoms break C-C bonds because C-H bonds are stronger than C-O bonds, inhibiting the formation of carbon chains that constitute sugars.

Finally, the abundance also decreases at $\text{H}/\text{C} \lesssim 2$ even if $\text{H}/\text{O} \approx 2$. When both H/C and H/O are low, carbon atoms tend to combine with each other, leading to the generation of open or cyclic carbon chains, and most of the large molecules existing in the UV phase contain many carbon atoms. After UV irradiation is finished, they keep the main structures because they already have many C-C bonds and few C-H bonds, and only oxygen atoms bonded to carbon chains are separated. Accordingly, they do not pass sugar molecules with $\text{O}/\text{C} = 1$.

3.4. Comparison with Meinert et al. (2016)'s Experiment

Meinert et al. (2016) mentioned that it is not clear when the ribose synthesis occurred in their experiments, in which they per-

form UV irradiation at 78 K followed by the transfer to the room temperature environment. Our simulation in this paper suggests that the dominant synthesis occurred at the room temperature after UV irradiation, although the synthesis pathway in our simulation (formation of O-rich molecules during UV irradiation followed by the break-ups of O-O bonds and replacements of -OH by -H at the room temperature) is totally different from formose-type building-up reactions suggested by Meinert et al. (2016) in most cases.

Because Meinert et al. (2016) also reported sugar alcohols (derivatives of sugars) in their products, we also examine the abundance of sugar alcohols in the simulation with initial species of 7 CH_3OH (methanol) and 20 H_2O that is similar to their experiments. We set $T_U = 10^5$ K and $T_p = 300$ K. The result is shown in Fig. 14. The abundance ratio of 5-C sugar alcohols to 5-C sugars is $R_{\text{al}} \approx 6.2$ at the peak in the post UV phase ($n_{\text{step}} = 78$). The ratio found in Meinert et al. (2016)'s experiment is $R_{\text{al}} \approx 4.1$, which is comparable to our simulation result.

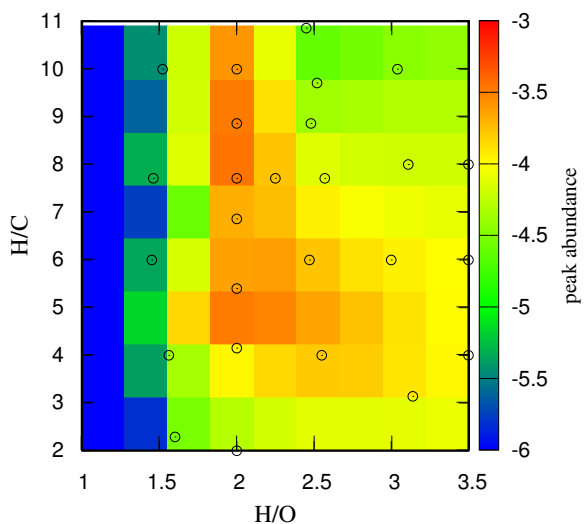


Fig. 11. The peak value of sugar abundance in the post UV phase for different element ratios of starting materials. The horizontal axis is the H/O ratio, and the vertical axis is the H/C ratio. The color bar indicates the peak value with a logarithmic scale; the red color means a large value.

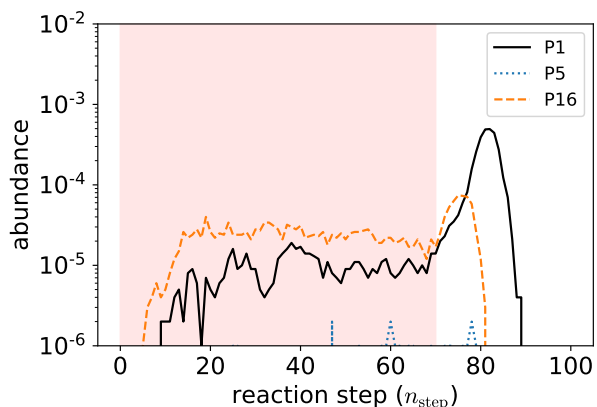


Fig. 12. Abundance of 5-C sugar as a function of a reaction step in the simulations for P1, P5, and P16 when $T_U = 10^5$ K, $T_p = 300$ K and $n_{\text{run}} = 10^6$. The black solid, blue dotted, and orange dashed lines represent the results for P1, P5, and P16, respectively.

3.5. Synthesis of Deoxysugars

Another experiment on sugar synthesis by UV irradiation (Nuevo et al. 2018) reported that deoxysugars were detected from the products and the abundance ratio of 5-C deoxysugars to 5-C sugars is $R_{\text{dxy}} \sim 1$. The abundance ratio in our simulation starting from 10 CH_3OH (methanol) and 20 H_2O , which is similar to Nuevo et al. (2018)’s experiment, with $T_U = 10^5$ K and $T_p = 300$ K shows $R_{\text{dxy}} \sim 1$ in entire steps (Fig. 15).

It is known that deoxysugars are not formed via formose-type reactions (Butlerow 1861; Breslow 1959). The detection of their derivatives, such as deoxysugar alcohols, in meteorites was reported (Cooper et al. 2001; Nuevo et al. 2018). Possible step-by-step building-up type pathways of deoxysugars synthesis were suggested in previous studies (Oró & Cox 1962; Ritson & Sutherland 2014). While the previously proposed synthesis pathways for sugars and deoxysugars are independent of each

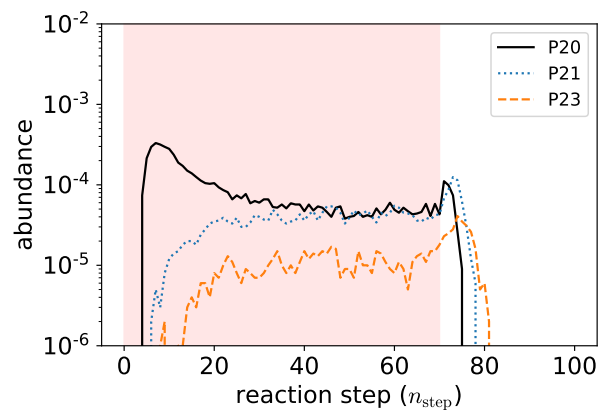


Fig. 13. Same as Fig. 12 except for P20, P21, and P23 instead of P1, P5 and P16.

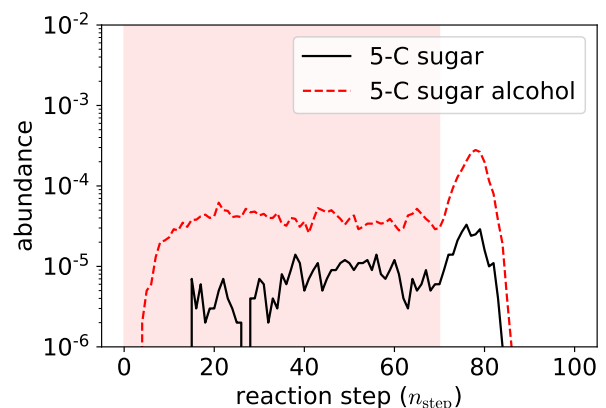


Fig. 14. Abundances of 5-C sugars and 5-C sugar alcohols as a function of a reaction step for set P5. The black solid and red dashed lines are for 5-C sugar and 5-C sugar alcohol, respectively.

other, the pathway shown in our simulations can simultaneously produce sugars and deoxysugars. As we argued in Sect. 3.1.2, in our simulations, the sugar synthesis occurs on the way of decomposition process at 300 K from large O-rich molecules generated during the UV phase to C-rich molecules. Our results show that sugars are synthesized not by a single unique path but by probabilistic, divergent paths. In other words, the synthesis paths have a “broad” range in phase space, compared with the conventional formose-type reactions. Because the structure of 5-C deoxysugars is similar to 5-C sugars and their synthesis probabilistically occurs, it is reasonable that their abundance is always similar to each other, almost independent of environmental conditions. The broad range enables the simultaneous synthesis of sugars, deoxysugars, and other related molecules. Because the cyclic form of deoxysugars would also be more stable, the same argument of preservation may be applied for deoxysugars.

4. Discussion

4.1. Activation Energy

In the Monte Carlo simulation in the present paper, we use the weighting factor $W' = \exp(-\Delta D/RT)$ (Eq. (4)) that does not depend on the activation energy E_a , instead of the more accurate weighting with $W = \exp(-E_a/RT)$ (Eq. (1)). During the UV

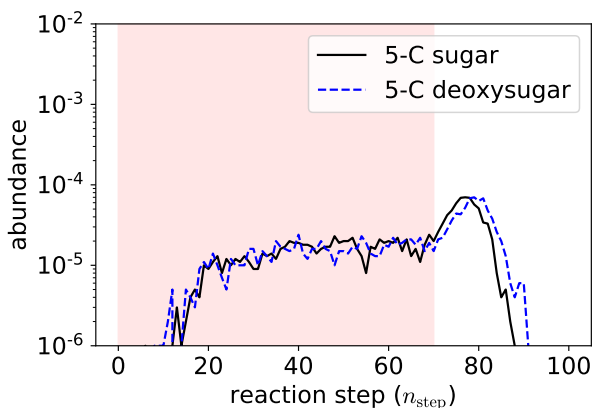


Fig. 15. Abundances of 5-C sugars and 5-C deoxysugars as a function of a reaction step. The black solid line and blue dashed line indicate 5-C sugar and 5-C deoxysugar, respectively.

phase, $E_a \ll RT$ with $T \sim 10^5$ K and all the minimum bond change reactions occur with the same probability, independent of E_a (Sect. 2.3). In the post UV phase where UV irradiation is turned off and $T = 300$ K is set, reactions of breaking up unstable large molecules with $\Delta D \sim -350$ to -260 kJ mol⁻¹ are repeated until sugar synthesis is peaked (Sect. 3.1.2). The Evans-Polanyi's empirical law, $E_a \approx \alpha \Delta D + \beta$ (Eq. (3)) where $\alpha \sim 0.6$ – 1 and $\beta \sim 100$ – 200 kJ mol⁻¹, suggests that E_a is negligible (E_a is $\lesssim 0$ kJ/mol), which is too small to induce an energy barrier in this case. The unstable O-rich large molecules are formed by UV irradiation and they play an important role in enhanced synthesis of sugars/deoxysugars in the post UV phase. Therefore, as long as we are concerned with the peaked abundance of sugars/deoxysugars, the effect of the activation energy should be negligible and it is justified to use W' as the weighting factor.

However, as noted in Sect. 2.2, for the reaction to actually occur, $E_a \lesssim 80$ kJ/mol is required at 300 K, which is equivalent to $\Delta D \lesssim -20$ to -120 kJ/mol for $\alpha \sim 1$. For the decomposition reactions of sugars/deoxysugars by replacement of -OH by -H, $\Delta D \approx -85$ kJ mol⁻¹. The reactions after the peaked synthesis of sugars/deoxysugars have ΔD with smaller absolute values (Fig. 8). It is not clear the reactions after the peaked sugars/deoxysugars synthesis proceeds at 300 K. This could contribute to the longer preservation of sugars/deoxysugars. The assumptions of our simulations are consistent with the “warm” environment of $T \sim 50$ – 100 K. In this case, the sugars/deoxysugars preservation should be further longer.

In summary,

1. UV phase:
The effect of E_a is negligible by the high equivalent T of UV irradiation ($E_a \ll RT$).
2. Early post UV phase until the peaked sugar/deoxysugar synthesis:
The effect is negligible for the repeated reactions with $\Delta D \sim -350$ to -260 kJ mol⁻¹ ($E_a \lesssim 0$).
3. Later post UV phase after the peaked synthesis:
The effect cannot be neglected, but its inclusion would prolong the preservation of sugars/deoxysugars, which is rather more consistent with our arguments.

Therefore, the effect of E_a would not significantly change the results in this paper.

To study the effect of the activation energy in more details, we need to perform quantum chemistry calculations or use

chemical reaction data bases². Because key reactions in the later post UV phase are limited, it may not be too difficult, although we leave it for future study.

We also point out in Sect. 3.1.3 that the transformation sugars/deoxysugars from the open-chain form to the cyclic form may contribute to the preservation of sugars/deoxysugars. More detailed discussions on bond energy originated from the three-dimensional structure of the molecules, which we do not take into account in the present paper, are also needed.

4.2. Synthesis of IOM-like Molecules

The mechanism found by our simulation simultaneously synthesizes sugars and deoxysugars. It could be consistent with the co-existence of sugars and deoxysugar derivatives in meteorites and the co-synthesis of sugars and deoxysugars found by a photochemistry experiment (Nuevo et al. 2018).

On the other hand, our simulation (Fig. 8 a) suggests that most of the molecules, which do not pass the sugars or deoxysugars, repeatedly suffer the reaction of C-H + C-OH \rightarrow C-C + H₂O with $\Delta D \approx -40$ kJ mol⁻¹ (Table 1). It decreases H/C at $n_{\text{step}} \gtrsim 80$ (Fig. 8 b), in addition to the steady decrease in O/C in the entire period of the post UV phase (Fig. 8 c). The final products are large C-rich molecules³.

In Fig. 8 b, the light and dark color dots represent the result with and without the prohibition of three or four-membered ring structures, respectively. In general, three or four-membered ring structures are unstable, because the wave functions of the atoms in the ring overlap. In our simulations, the formation of three or four-membered ring structures is prohibited. Following this prescription, H/C \rightarrow 1.7 and O/C \rightarrow 0.86 (the light color dots). However, we find that due to the limitation of only 7 carbon atoms in the simulations with the prohibition of three or four-membered ring structures, complex carbon rings with several -OH groups remain. In reality, carbon atoms are almost infinite, and more C-rich molecules with smaller H/C and O/C are likely to be formed. We also performed runs with the same initial molecules and the same random number sequences without the prohibition of three or four-membered ring structures (the dark color dots). Until the sugar synthesis, the distributions of H/C and O/C are almost the same as those with the prohibition. After the sugar synthesis, however, more C-rich final products with lower H/C and O/C are formed. The final molecules have multiple combinations of three and four-membered ring structures. In reality, stable molecules with multiple combinations of five and six-membered ring structures would be formed.

These theoretically inferred final products have structures similar to the complex Insoluble Organic Matter (IOM) that is a major component in organic matters in carbonaceous chondrites (Derenne & Robert 2010). The molecule distribution in carbonaceous chondrites that includes sugars, deoxysugars, Soluble Organic Matter (SOM), and IOM may be inconsistent with the conventional building-up type synthesis (Isa et al. 2021). However, the synthesis model proposed in our present paper could be con-

² In our prescription, any reaction is divided into the sum of the minimum bond change reactions and the transition state is partially taken into account in some cases. For example, ammonia formation from N₂ is divided into three reactions, N₂+3H₂ \rightarrow N₂H₂+2H₂ \rightarrow 2NH₂+H₂ \rightarrow 2NH₃. For the whole reaction of N₂+3H₂ \rightarrow 2NH₃, $\Delta H < 0$. However, for the first and second reactions, $\Delta H > 0$, implying that the divided states of N₂H₂ + 2H₂ and 2NH₂ + H₂ express energy barriers.

³ When hydrogen excess is substantial, some carbon atoms are combined with hydrogen atoms and produce methane, which is mentioned in Section 3.3.

sistent with the organic molecule distribution in carbonaceous chondrites. Detailed comparison of the theoretical prediction with the distribution of organic matter species (sugars, deoxy-sugars, amino acids, their derivatives, and IOM) is left for future study⁴.

5. Conclusions

In order to investigate photochemistry by intermittent UV irradiation on the surface of icy particles in the protoplanetary disk, we have developed a new Monte Carlo code to simulate reaction sequences of organic molecules, using a graph-theoretic matrix model. Our model does not assume a chemical reaction network in advance. Instead, 1) we list up all the possible reactions at every step, 2) select one of the reactions with a weighting factor depending on the bond energy change and temperature, assuming a warm environment where all the species can interact with one another without spatial separation, 3) and repeat this process to follow a reaction sequence.

We tested 26 patterns of starting molecules with the fiducial case of 7 CH₂O and 20 H₂O. For each pattern, we have performed 10⁵–10⁶ Monte Carlo simulation runs consisting of a reaction sequence of 70 UV phase steps and 30 post UV phase steps, considering icy dust particles that occasionally diffuse to an upper disk region and are exposed to UV radiation from a host star (Figure 2).

We focused on the analysis of the synthesis of 5-C sugars (ribose) and related molecules such as deoxysugars. We have found that our simulation results would be consistent with the past UV photochemistry experiments to synthesize ribose/deoxyribose and the organic molecules in carbonaceous chondrites, however, through a different pathway from the conventional step-by-step formose-type reactions that have been suggested by the past studies, as illustrated in Fig. 4. Our results are summarized as follows.

1. Sugar abundance rapidly increases after UV irradiation is turned off. Ribose (5-C sugars) and 4-C sugars show the similar evolution except for a slightly higher abundance for 4-C sugars. The peak abundance values are not affected by UV photon energy (E_{UV}) and the temperature (T_p) at the post UV phase, as long as $E_{UV} \gtrsim 1$ eV (the equivalent temperature is $T_U \gtrsim 10^4$ K) and $T_p \lesssim 10^3$ K.
2. During the UV phase, loosely-bonded O-rich large molecules are continuously created and destroyed. In the post UV phase, these molecules are unstable and decomposed by reactions cleaving O-O bonds and replacing C-OH by C-H, toward stable structures. Molecule sizes become smaller with decreasing O/C. Some fraction of the decaying molecules form sugars with O/C = 1 and H/C = 2. We argue that the sugars should be stabilized by transformation to the cyclic form.
3. Our results would be consistent with the past UV photochemistry experiments and carbonaceous chondrites. However, the sugar synthesis pathway in our results contrasts with the previously suggested formose-type reactions where the molecular size grows step by step and molecules at every step are stable at room temperature.
4. The synthesized ribose abundance does not depend on specific forms of starting molecules, but is regulated mostly by H/O ratios of total starting molecules. The abundance is

peaked at H/O \approx 2, such as a set of formaldehyde (CH₂O) and water molecules (H₂O).

5. Ribose and deoxyribose are simultaneously synthesized with similar abundance, which is consistent with the past experimental results (deoxyribose is not produced via formose-type reactions). Because the distribution generated by UV irradiation includes divergent molecules and chemical structures of ribose and deoxyribose are similar, it is reasonable that their abundances are also similar.

Our simulation suggests that most of the molecules finally become complex C-rich molecules, which is similar to IOM, the major component of organics in carbonaceous chondrites. The co-synthesis of ribose and deoxyribose we found may also be consistent with the chondrites. Detailed comparison with carbonaceous chondrites as well as with experiments is left for future study.

Acknowledgements. We thank the referee for helpful comments to improve the manuscript. Because this research is a new challenge for us, we have had a lot of discussions with many colleagues. We thank Hiroshi Naraoka, Yoshihiro Furukawa, Yasuhiro Sekine, and Junko Isa for comments from cosmochemistry, Ryuhei Nakamura for comments from chemistry, Yuri Aikawa, Hideko Nomura, and Kenji Furuya for comments from theoretical astrochemistry, Satoshi Yamamoto and Nami Sakai for comments from observations of interstellar organic molecules, Hiroshi Kobayashi, Seiichiro Watanabe, Yuka Fujii, and Masahiro Ogihara for insightful theoretical discussions. We also thank Kimito Funatsu, Masashi Aono, Yoshi Oono, and Yu Komatsu for helpful advice for developing the new scheme presented here. This research is supported by JSPS Kakenhi 21H04512, MEXT Kakenhi 18H05438, and MEXT “Program for Promoting Researches on the Supercomputer Fugaku” (From clouds to stars and planets: toward a unified formation scenario).

References

- Alibert, Y., Carron, F., Fortier, A., et al. 2013, *A&A*, 558, A109
- Armitage, P. J. 2013, *Astrophysics of Planet Formation*
- Azofra, L. M., Alkorta, I., Elguero, J., & Popelier, P. L. 2012, *Carbohydrate Research*, 358, 96
- Benz, W., Ida, S., Alibert, Y., Lin, D., & Mordasini, C. 2014, in *Protostars and Planets VI*, ed. H. Beuther, R. S. Klessen, C. P. Dullemond, & T. Henning, 691
- Bergner, J. B. & Ciesla, F. 2021, *ApJ*, 919, 45
- Breslow, R. 1959, *Tetrahedron Letters*, 1, 22
- Butlerow, A. 1861, *Justus Liebigs Annalen der Chemie*, 120, 295
- Chang, Q. & Herbst, E. 2016, *The Astrophysical Journal*, 819, 145
- Chyba, C. & Sagan, C. 1992, *Nature*, 355, 125
- Ciesla, F. J. & Sandford, S. A. 2012, *Science*, 336, 452
- Cooper, G., Kimmich, N., Belisle, W., et al. 2001, *Nature*, 414, 879
- Cooper, G. & Rios, A. C. 2016, *Proceedings of the National Academy of Science*, 113, E3322
- Dass, A. V., Georgelin, T., Westall, F., et al. 2021, *Nature Communications*, 12, 2749
- Derenne, S. & Robert, F. 2010, *Meteoritics and Planetary Science*, 45, 1461
- Dugundji, J. & Ugi, I. 1973, *Computers in Chemistry*, 19
- Furukawa, Y., Chikaraishi, Y., Ohkouchi, N., et al. 2019, *Proceedings of the National Academy of Sciences*, 116, 24440
- Garrod, R. T. 2019, *ApJ*, 884, 69
- Habershon, S. 2015, *J Chem Phys*, 143, 094106
- Habershon, S. 2016, *Journal of Chemical Theory and Computation*, 12, 1786, PMID: 26938837
- Ida, S. & Lin, D. N. C. 2004, *ApJ*, 604, 388
- Ida, S. & Lin, D. N. C. 2005, *ApJ*, 626, 1045
- Ida, S. & Lin, D. N. C. 2010, *ApJ*, 719, 810
- Ida, S., Lin, D. N. C., & Nagasawa, M. 2013, *ApJ*, 775, 42
- Isa, J., régis Orthous-Daunay, F., Beck, P., et al. 2021, *The Astrophysical Journal Letters*, 920, L39
- Ismail, I., Stuttaford-Fowler, H. B. V. A., Ochan Ashok, C., Robertson, C., & Habershon, S. 2019, *Journal of Physical Chemistry A*, 123, 3407
- Jin, M. & Garrod, R. T. 2020, *The Astrophysical Journal Supplement Series*, 249, 26
- Kim, Y., Kim, J. W., Kim, Z., & Kim, W. Y. 2018, *Chem. Sci.*, 9, 825
- Limão-Vieira, P., Eden, S., Mason, N., & Hoffmann, S. 2003, *Chemical Physics Letters*, 376, 737–747

⁴ When the final products are discussed, the effect of the activation energy need to be taken into account as discussed in Sect. 4.1.

Martins, Z., Botta, O., Fogel, M. L., et al. 2008, *Earth and Planetary Science Letters*, 270, 130

Martins, Z., Modica, P., Zanda, B., & D'Hendecourt, L. L. S. 2015, *Meteoritics & Planetary Science*, 50, 926

Meinert, C., Myrgorodska, I., de Marcellus, P., et al. 2016, *Science*, 352, 208

Michaelides, A., Liu, Z.-P., Zhang, C. J., et al. 2003, *Journal of the American Chemical Society*, 125, 3704, PMID: 12656593

Miller, S. L. 1953, *Science*, 117, 528

Miller, S. L. 1955, *Journal of the American Chemical Society*, 77, 2351

Mordasini, C., Alibert, Y., & Benz, W. 2009, *A&A*, 501, 1139

Nuevo, M., Cooper, G., & Sandford, S. A. 2018, *Nature Communications*, 9, 5276

Okamoto, T. & Ida, S. 2022, arXiv e-prints, arXiv:2201.05507

Oró, J. 1961, *Nature*, 190, 389

Oró, J. & Cox, A. 1962in , *FEDERATION AMER SOC EXP BIOL* 9650
ROCKVILLE PIKE, BETHESDA, MD 20814-3998, 80

Ritson, D. J. & Sutherland, J. D. 2014, *Journal of Molecular Evolution*, 78, 245

Rzepa, H. S. 2021, *Nature Communications*, 12

Saitta, A. M. & Saija, F. 2014, *Proceedings of the National Academy of Science*, 111, 13768

Sanderson, R. 1976, *Chemical bonds and bonds energy*, Vol. 21 (Elsevier)

Sato, T., Okuzumi, S., & Ida, S. 2016, *A&A*, 589, A15

Sorrell, W. H. 2001, *ApJ*, 555, L129

Sutton, J. E. & Vlachos, D. G. 2012, *ACS Catalysis*, 2, 1624

Tachibana, S., Kouchi, A., Hama, T., et al. 2017, *Science Advances*, 3, eaao2538

Wang, L.-P., Titov, A., McGibbon, R., et al. 2014, *Nature Chemistry*, 6, 1044

Wang, S., Temel, B., Shen, J., et al. 2011, *Catalysis Letters*, 141, 370